

05,13

Investigation of optically induced formation of magnon zones in the structure of YIG|periodic gallium arsenide

© K.V. Bublikov¹, S.E. Sheshukova², E.N. Beginin², M. Tapajna¹, D. Gregušová¹, S.N. Krylov^{1,2}, A.I. Stogniy³, S. Korchagin¹, S.A. Nikitov^{2,5}, A.V. Sadovnikov²

¹ Institute of Electrical Engineering, Slovak Academy of Sciences, Bratislava, 841 04 Slovakia

² Saratov National Research State University, Saratov, Russia

³ Scientific and Practical Materials Research Center, National Academy of Sciences of Belarus, Minsk, Belarus

⁴ Financial University under the Government of the Russian Federation, Moscow, Russia

⁵ Kotelnikov Institute of Radio Engineering and Electronics, Moscow, Russia

E-mail: elekbubl@savba.sk

Received April 17, 2023

Revised April 17, 2023

Accepted May 11, 2023

The present work is devoted to the study of the optically induced formation of the band structure of a magnon crystal consisting of a ferrite microwave diode loaded with a semiconductor with periodic thickness modulation. Using the Brillouin light scattering method, it is demonstrated that an increase in the power of laser radiation illuminating the semiconductor layer leads to the formation of non-transmission bands in the spectrum of surface magnetostatic waves (PMSW) with a simultaneous increase in the central frequency of these bands. Using the finite element method, we connected the formed non-transmission bands with the Bragg resonances of the periodic structure, and also evaluated the effect of changes in the density of semiconductor electrons on the dispersion dependences and non-reciprocal properties of PMSV in such a structure.

Keywords: spin waves, magnonics, semiconductor magnonics, magnonic crystals, layered structures.

DOI: 10.61011/PSS.2023.07.56399.32H

1. Introduction

Magnonics is a discipline that emerged about ten years ago as further development of spintronics and spin-wave electronics [1–4]. Compared with electron-transfer process technology — CMOS (complementary metal oxide semiconductor), magnonics is a field of physics investigating physical processes associated with generation, propagation and interaction of spin waves (SW) in magnetic structures [5,6]. Currently, the purpose of magnonics is to develop base elements capable of forming integrated circuit and of replacing/supplementing/expanding, by overcoming the CMOS electronics limitations, the functionality of the existing CMOS devices [3,7,8].

Magnonic crystals (MC) — periodic magnetic structures allowing to form/change spectra of SW going through the structure due to the presence of non-transmission bands — are of high interest for magnonics [9,10]. The possibility of development of rearrangeable MC with variable non-transmission band width and arrangement offers great opportunities of creating magnonic-based signal processing devices. The transfer characteristic rearrangement methods include direct exposure in order to modify material characteristics of a magnetic microwaveguide — for example,

by optically-induced heating [11,12] or using current/voltage by means of produced electrodes [13,14]; or indirect interaction by using laminar structures (e.g. using a ferroelectric layer [15], superconducting layer [16], piezoelectric layer [17]).

A separate task includes the development of so-called dynamic magnonic structures (including MC) where typical transfer characteristic changeover time is comparable with the operating frequency of a device (GHz and THz for spin waves [1]). Also, when developing a rearrangeable MC, an approach is interesting which would enable the periodic lattice to be changed during the device operation in order to expand its functional properties.

This study evaluates the possibility of using a multilayer consisting of yttrium-iron garnet (YIG) and gallium arsenide (GaAs) for creation of optically rearrangeable magnonic crystal. Change of spin wave properties in semiconductor-loaded structures due to optically induced change of charge carriers in the semiconductor was demonstrated, for example, in [18–21]. These effects are qualitatively similar to occurrence of nonreciprocal properties of magnetostatic surface waves (MSSW) in MC loaded in the form of a metal layer [22] and in MC with periodic lattice formed

by metal bands over a magnetic microwaveguide [22]. High interest to the YIG|GaAs multilayer shall be pointed out due to the recent studies regarding growing of YIG submicron films on gallium arsenide substrates [19,23] to offer opportunities of integrating magnonic elements into the existing CMOS devices. Also, the semiconductor layer is advantageous in terms of creating a space- and time-varying periodic MC lattice by optical induction of charge carriers. In addition, the rate of change of such periodic lattice is limited by optical generation and charge carrier recombination processes in the semiconductor layer [24,25] which is potentially sufficient for the development of dynamic magnonic devices.

The aim of this study is to investigate formation of band structure of a magnonic crystal consisting of YIG microwaveguide loaded with a GaAs plate with periodic grooves on the surface oriented towards the YIG layer. When such semiconductor surface was exposed to laser light, the periodic lattice contrast enhancement of the produced magnon crystal was expected (due to increased concentration of charge carriers in GaAs). By means of measurements using Brillouin light scattering (BLS) method [26], we have demonstrated that the power growth of laser emission illuminating the semiconductor layer is followed by formation of non-transmission bands in the MSSW spectrum: frequency range and absorption increased and also the band center frequency was growing. Using numerical electrodynamic modeling of structure model eigenwaves, we demonstrated the relationship between the occurring non-transmission bands and Bragg resonances, and variation of their frequency with increasing electron concentration in the semiconductor layer and followed by occurrence of nonreciprocal effect of magnetostatic surface waves in the structure.

2. Structure and numerical investigation

The diagram of the produced structure is shown in Figure 1. The magnetic microwaveguide 1 mm in width and 20 mm in length was formed by laser ablation from 9 μm YIG film grown by the liquid-phase epitaxy method on a gallium-gadolinium garnet (GGG) substrate. The YIG film had the following parameters: dielectric constant $\varepsilon = 9$, gyromagnetic ratio $\Upsilon = 2.8 \text{ mHz/Oe}$ [27], saturation magnetization $4\pi M_S = 1750 \text{ G}$ (sample nameplate rating), ferromagnetic resonance width $\Delta H = 0.54 \text{ Oe}$ measured at 9.7 GHz (sample nameplate rating).

Above the produced microwaveguide, a GaAs plate 1 mm in width, 500 μm in thickness and 5 mm in length was attached. This GaAs plate consisted of a 1 μm heavily doped *n*-GaAs layer on the surface of 499 μm *n*-type semi-insulator layer. After production of 4 ohmic contacts on each side of the plate, two-dimensional resistivity was measured on both sides of the sample without laser illumination. This allowed to determine electrical conductivity: $6.41 \cdot 10^{-7} \text{ S/cm}$ for the lightly doped side and $1.35 \cdot 10^3 \text{ S/cm}$ for the heavily

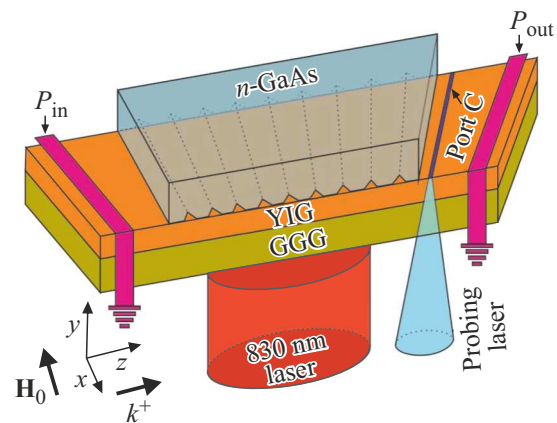


Figure 1. Diagram of the studied structure (proportions are not obtained) consisting of *n*-type (*n*-GaAs) gallium arsenide plate secured above the yttrium-iron garnet (YIG) microwaveguide on the gallium-gadolinium garnet (GGG) substrate. The structure was exposed to control laser emission (830 nm laser), the beam center was focused to the GaAs plate center in *x*–*z* plane. The inlet and outlet antennas of the microwave signal microstrip converters are designated as P_{in} and P_{out} , respectively. Along port C line, Mandelstam–Brillouin light scattering investigation was carried out using probing laser beam.

doped side. Ignoring the hole conductivity of the sample, drift electron mobility, μ_e (hereinafter referred to as the electron mobility) and electron concentration, N_e , pairs corresponding to the measured conductivity were matched according to the dependence of electron mobility in GaAs on electron concentration associated with doping (see [28]). Thus, without laser illumination, the electron mobility and concentration for the lightly doped side were determined as $N_e = 1 \cdot 10^9 \text{ cm}^{-3}$, $\mu_e = 8400 \text{ cm}^2/(\text{Vs})$, for heavily doped side — as $N_e = 1 \cdot 10^{18} \text{ cm}^{-3}$, $\mu_e = 4000 \text{ cm}^2/(\text{Vs})$, that corresponds to typical values for GaAs with corresponding doping [29,30]. On the heavily doped side of the plate further facing the YIG layer, V-shaped grooves 100 μm in depth and 70 μm in width at the GaAs surface were made by the laser ablation method with period $D = 200 \mu\text{m}$.

To convert the incoming microwave signal into spin waves (and for their detection), the structure was secured on the holder with two 30 μm microstrip antennas spaced at 9 mm. The holder with the sample was placed in $H_0 = 900 \text{ Oe}$ bias field oriented tangentially to the sample surface and perpendicularly to the wave propagation ($\mathbf{H}_0 \parallel x$, see Figure 1) to ensure excitation of magnetostatic surface waves (so-called Damon–Eshbach configuration [6,27,31]). For optical induction of non-equilibrium charge carries in the GaAs plate, we used „control laser“ — a 830 nm optical fiber laser illuminating the structure on the optically transparent GGG and YIG sides. Without any structure, dimensions of the elliptical laser spot at such distance from the emitter as in this experiment were equal to $9 \times 6 \text{ mm}$. The calibrated optical power of the laser beam P_L varied within 0–300 mW. The authors were not able to determine

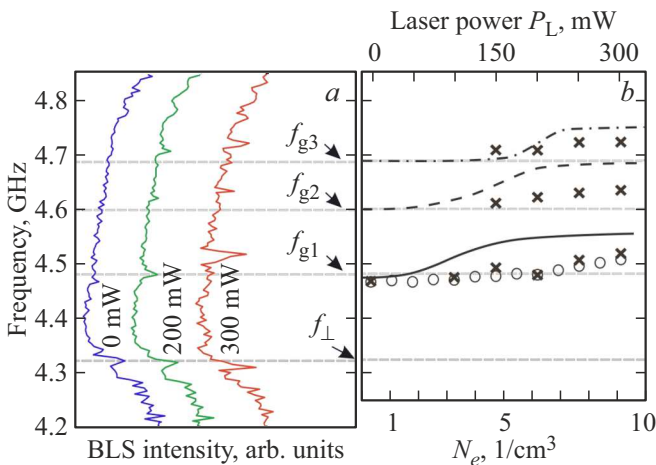


Figure 2. *a)* Dependences of frequency vs. BLS signal intensity in the studied structure using $P_L = 0, 200$ and 300 mW control laser power. Frequencies for wave numbers of the first three Bragg resonances of MSSW obtained using the Damon–Eshbach model (without GaAs) are designated as f_{g1}, f_{g2} and f_{g3} . The ferromagnetic resonance frequency obtained from the BLS signal measured for the non-exposed structure is designated as f_{\perp} . *b)* Crosses: frequencies of the first three Bragg resonances obtained from the BLS signal depending on the laser power P_L . Circles: frequency of the first Bragg resonance obtained from AFC depending on the laser power P_L . Curves show the dependences of Bragg resonance frequencies (solid line — the first resonance, dashed line — the second resonance, dashed-dotted line — the third resonance) on the gallium arsenide electron density (N_e) calculated by the finite element method.

experimentally the dependences of charge carrier mobility and concentration on the GaAs plate sides with varying laser power. However, the expected increase in the carrier concentration is about 1.5 orders of magnitude from the initial value [24,25]. It should be noted that due to the difference in electron and hole mobility during laser exposure, the change in the hole concentration in the GaAs plate was neglected.

BLS measurement [26] was carried out along port C line (see Figure 1) with step 25 nm and the distance between the exciting antenna and port C was equal to 7.5 mm. For the measurement, EXLSR-532-200-CDRH 532 nm and 1 mW single-frequency probing laser was used (see Figure 1). The laser beam was focused on the YIG surface and was 25 μ m in diameter. Measurement configuration allowed to achieve a BLS signal proportional to the tangential dynamic component of magnetization in the YIG film in the region exposed to the probing laser. Whilst the measurements were carried out for MSSW excited by the inlet antenna P_{in} . After integration of BLS spectra measured along port C line, frequency dependences of BLS signal (BLS spectra) similar to MSSW amplitude-frequency characteristics (AFC) were obtained.

Figure 2, *a* shows the measurements of frequency vs. BLS signal at different control laser powers P_L . Dashed line f_{\perp}

shows the dip frequency on the BLS signal spectrum (measured without the control laser emission) corresponding to the ferromagnetic resonance. Dependences of frequency vs. BLS signal allow to observe whether alternating transmission bands and non-transmission bands are present in the spin wave spectrum (corresponding to dips in the BLS signal amplitude). Due to the fact that non-transmission bands on the BLS spectrum at $P_L = 0$ mW are poorly distinguishable/non-distinguishable, the expected frequency positions of the Bragg resonances were determined for this structure. Non-transmission bands in the periodic structures are associated with the Bragg resonances between the waves going through the structure (k^+) and waves reflected from the periodic lattice (k^-) [9]. Generally, a Bragg band gap is formed when the frequencies of such oppositely directed waves become equal and wave numbers correspond to the general condition of the Bragg resonance

$$|k_B^-| + |k_B^+| = m \frac{2\pi}{D}, \quad (1)$$

where D is the structure period, k_B is the Bragg resonance wave number for transmitted and reflected waves, m is the Bragg resonance order (positive integer). In case when the dispersion law is invariant for oppositely directed waves (wave nonreciprocity is absent), $|k_B^-| = |k_B^+|$, and (1) turns into the Bragg resonance condition for structures without wave nonreciprocity

$$k_B = m \frac{\pi}{D}, \quad (2)$$

where k_B is the wave number of m -order Bragg resonance for structures without wave nonreciprocity. Thus, if the wavelengths corresponding to m -Bragg resonance differ from those calculated in (2), then the Bragg resonance occurs between nonreciprocal waves k^+ and k^- .

Substituting k_B for $m = 1, 2, 3$ (157.08, 314.159, 471.239 cm^{-1} , respectively) into the Damon–Eshbach dispersion law, we obtain frequencies $f_{g1} = 4.482$ GHz, $f_{g2} = 4.6$ GHz, $f_{g3} = 4.688$ GHz shown in Figure 2.

Now, it can be suggested that the BLS signal dip at 4.468 GHz in the BLS spectrum at $P_L = 0$ is associated with the first Bragg resonance in the structure of interest. Designate m -order Bragg resonances determined from the BLS spectra as $\text{bgm}(P_L)$, and their frequencies, respectively, as: $f_{\text{bgm}}(P_L)$. Frequency $f_{\text{bg1}}(0) = 4.468$ GHz was below f_{g1} . This may be explained by the influence of the lateral dimension of the waveguide structure (compared with the Damon–Eshbach model for the plane-infinite layer) and formation of the MSSW transverse mode spectrum in the propagating wave process [32]. It should be noted that the BLS signal dips corresponding to the Bragg resonances higher than $m = 1$ cannot be distinguished at the existing signal-to-noise ratio for the measured dependence of BLS signal on frequency at $P_L = 0$.

The BLS spectrum at $P_L = 200$ mW has three clearly seen dips near f_{g1}, f_{g2} and f_{g3} , consider that they

correspond to three Bragg resonances:

$$f_{bg1}(200 \text{ mW}) = 4.481 \text{ GHz},$$

$$f_{bg2}(200 \text{ mW}) = 4.4622 \text{ GHz},$$

$$f_{bg3}(200 \text{ mW}) = 4.732 \text{ GHz}.$$

In this case, the width and depth of $bg1(200 \text{ mW})$ dip increased compared with the BLS spectrum at $P_L = 0$, and the mean frequency of this dip increased. Dip frequencies $f_{bg2}(200 \text{ mW})$ and $f_{bg3}(200 \text{ mW})$ are higher than f_{g2} and f_{g3} . With further increase in the laser power ($P_L = 300 \text{ mW}$), the width and depth of the produced non-transmission bands are higher compared with the spectrum at $P_L = 200 \text{ mW}$. Dip frequency $f_{bgm}(300 \text{ mW})$ is also higher compared with the spectrum at $P_L = 200 \text{ mW}$. Thus, it should be noted that three Bragg band gaps are detected on the BLS spectra at $P_L = 200$ and 300 mW . Also, it can be suggested that the Bragg band gaps are formed in the studied structure with growing control laser power. Actually, we experimentally observe optical „inclusion“ of non-transmission bands in the MSSW spectrum.

The dip frequencies corresponding to the Bragg resonances on the BLS spectra are shown in Figure 2, *b* (crosses) as a function of power: $f_{bgm}(P_L)$. Figure 2, *b* shows that the dips corresponding to the Bragg resonances $m = 2$ and $m = 3$ were distinguished beginning from $P_L = 150 \text{ mW}$. Gradual growth of the Bragg band gap position frequency with growth of P_L .

Position of the first Bragg resonance with variation of P_L was also determined on the MSSW amplitude-frequency characteristics of the studied structure detected by the receiving antenna P_{out} (see Figure 1). It should be noted that the low signal level and high noise level in the measured AFC prevented detection of dips corresponding to the Bragg resonances higher than $m = 1$. However, due to the frequency-dependent sensitivity of the Bragg resonance in the studied structure to the control laser power variation, band gap frequency at $m = 1$ was possible. Frequency dependence of the band gap position of the first Bragg resonance vs. control laser power is shown in Figure 2, *b* (circles). Comparison of the band gap frequencies obtained from the BLS and AFC spectra show that these dependences are in good agreement. This comparison also proves that the measured Bragg resonance frequency $f_{bg1}(0)$ is correct (the value obtained from AFC is equal to 4.467 GHz).

Consider the MSSW dispersion dependences in the studied structure obtained from the phase-frequency characteristics measured at $P_L = 0$ and $P_L = 300 \text{ mW}$ (solid curves in Figure 3, *a* and *b*, respectively). Since no MSSW non-transmission band was actually formed for the first Bragg resonance in the non-exposed structure (see absorption peak $bg1(0)$ in Figure 2, *a*), the frequency jump typical for the non-transmission bands at a constant wave number (so-called shelf) is not visible on the experimental dispersion curve at $P_L = 0$ (considering the signal-to-noise ratio).

However, at the first Bragg resonance frequency obtained from AFC of the non-exposed structure (4.467 GHz), the measured dispersion curve has the wave number equal to π/D . According to (2), it can be assumed that MSSW nonreciprocity is absent at the MSSW wavelength corresponding to the first Bragg resonance (with the measurement accuracy defining the dispersion curve).

According to [33], occurrence of MSSW nonreciprocity in lamellar structures is associated with the wave skin layer thickness outside the magnetic layer. This thickness is defined by the effect of load on the electromagnetic field shielding of the wave and also is proportional to the wavelength. Thus, according to the experimental dispersion shown in Figure 3, *a*, the MSSW nonreciprocity is possible only for $k < \pi/D$.

At the dispersion curve measured experimentally at $P_L = 300 \text{ mW}$, the frequency jump (at frequencies near f_{bg1}) corresponding to the first Bragg resonance is observed at $k \approx 141.8 \text{ cm}^{-1}$. Thus, the Bragg resonance between nonreciprocal MSSW may be suggested; and the wave nonreciprocity is caused by the increasing control laser power. It should be also noted that displacement of the dispersion curve into the lower wave number and higher frequency region qualitatively corresponds to the studies devoted to the MSSW propagation in the semiconductor-loaded structures [18,21].

To understand the dependence of band structure of the GaAs|YIG type periodic magnon crystal on the semiconductor electron concentration, we used the numerical simulation by finite element method. The simulation diagram was similar to [22,33,34] and was based on the Helmholtz equation solution on the assumption that the wave number eigenvalues of quasi-TE waves (corresponding in the considered MSSW frequency range) obey the Bloch theorem. The structure eigenwave frequencies were determined at the predefined wave numbers. One structure period along direction z was considered, the model involved a homogeneous endless structure along direction x and endless number of periods along direction z . Magnetic properties of YIG were described by the gyromagnetic permeability tensor $\hat{\mu}$, semiconductor properties of GaAs were described by the permittivity tensor component ε_{zz} (similar to [21,35]):

$$\varepsilon_{zz} = \varepsilon_g + \frac{i\omega_p^2}{-\omega(i\omega + 1/\tau)}, \quad \omega_p = \sqrt{\frac{N_e q^2}{\varepsilon_0 m_e}}. \quad (3)$$

ε_g — is the crystal lattice contribution to permittivity, ω is the angular frequency, ω_p is the plasma frequency of semiconductor electrons, τ is the average semiconductor electron free path, N_e is the semiconductor electron density, q is the electron charge, ε_0 is the vacuum permittivity, m_{pe} is the effective electron mass in the semiconductor.

For the numerical simulation, only the influence of the highly doped gallium arsenide layer located at the air gap distance of $5 \mu\text{m}$ from the YIG surface was considered. The following constitutive parameters were used: $\varepsilon_g = 12.9$,

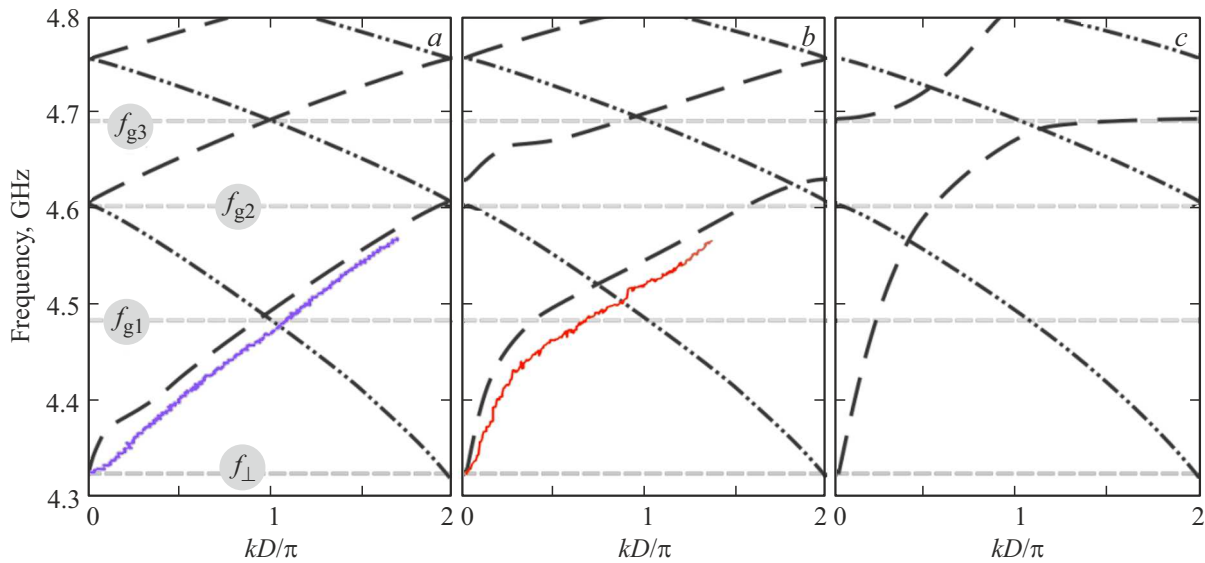


Figure 3. MSSW dispersion characteristics in the studied structure: experimental (solid lines), calculated by finite element method for $\mathbf{k} \uparrow z$ (dashed lines) and $\mathbf{k} \downarrow z$ (dashed-dotted lines). *a)* $P_L = 0$ mW, $N_e = 1 \cdot 10^{18} \text{ cm}^{-3}$. *b)* $P_L = 300$ mW, $N_e = 3.2 \cdot 10^{18} \text{ cm}^{-3}$. *c)* $N_e = 6.3 \cdot 10^{18} \text{ cm}^{-3}$. Frequencies for wave numbers of the first three Bragg resonances of MSSW obtained using the Damon–Eshbach model (without GaAs) are designated as f_{g1} , f_{g2} and f_{g3} . The ferromagnetic resonance frequency determined from the measured BLs signal for the non-exposed structure is designated as f_{\perp} .

$m_e = 0.13$ from the electron mass, $\tau = 0.296 \cdot 10^{-12}$ s (the value was defined from the electron mobility).

The dispersion relationships calculated for the eigenwaves by the finite element method at different electron concentrations in gallium arsenide are shown in Figure 3. Solutions for waves k^+ are shown by the dashed lines and for solutions k^- — by the dotted lines. Intersections of these solutions according to (1) define the frequencies and wave numbers of the Bragg resonances.

Electron concentration $N_e = 1 \cdot 10^{18} \text{ cm}^{-3}$ (dispersion for this concentration is shown in Figure 3, *a*) is equal to the measurement on the non-exposed heavily doped side of the GaAs sample. Intersections of solutions for transmitted and reflected waves correspond to the Bragg resonances defined by (2) (resonances for MSSW without nonreciprocity). It should be also noted that the Bragg resonance frequencies correspond to f_{g1} , f_{g2} and f_{g3} with good accuracy, which is explained by endless lateral dimension of the structure (along the x axis) in the numerical model. Significant difference in the dispersion law for waves k^+ and k^- (nonreciprocity manifestation) is observed only at $k < 80$ 1/cm that is caused by the enhanced role of semiconductor load in shielding of the MSSW electromagnetic fields with wavelength growth which agrees with [33].

Dispersion characteristics numerically assessed at electron concentration in gallium arsenide $N_e = 3.2 \cdot 10^{18} \text{ cm}^{-3}$ are shown in Figure 3, *b*. It should be noted that for the first two Bragg resonances, wave numbers are substantially different from law (2), which is indicative of the resonance between nonreciprocal MSSW. The dispersion law for waves k^- varied negligibly compared with the solution shown in Figure 3, *a*, while the dispersion wave characteristic k^+

moved to the high frequency and wavelength region according to the experimental data. The difference between numerical k^+ and experimentally measured dispersion laws is again expected due to the finite lateral dimension of the experimental sample.

Further increase in the electron concentration in GaAs in the numerical experiment (see Figure 3, *c*, $N_{pe} = 6.3 \cdot 10^{18} \text{ cm}^{-3}$) results in even greater shift of wave dispersion k^+ into the higher frequency and lower wave number region, while the first three Bragg resonances occur between the nonreciprocal MSSW. At the same time, the dispersion law for inverse waves (k^-) varied negligibly compared with that at the density of GaAs electrons $N_e = 1 \cdot 10^{18} \text{ cm}^{-3}$ (Figure 3, *a*).

It should be noted that the model do not show formation of dispersion gaps corresponding to the non-transmission bands of the Bragg resonances. This may suggest that some losses were not considered (for example, the losses associated with electron acceleration in the MSSW propagating field could have been not considered in the simulation based on the Boltzmann linearized kinetic equation that provides a solution in the form of semiconductor tensor $\hat{\varepsilon}$ [6,27]). Generally, due to the statement of eigenvalue problem in the form of search for solution of frequencies at the specified wave numbers, it is not possible to consider the spatial losses (defined by the imaginary component of the wave number) using the model. However, the model allows to predict variation of the Bragg resonance positions depending on the frequency.

To compare the experimental dependences $f_{bgm}(P_L)$ with the numerical simulation results, dependences $f_{bgm}(N_e)$ were defined from the numerically calculated dispersion

laws (see the curves in Figure 2, *b*). Qualitative similarity of the Bragg resonance frequency growth in the experiment and simulation should be noted. However, the gradual nature of dependences $f_{bgm}(P_L)$ is varies towards the S-shaped curves $f_{bgm}(N_e)$. The lower limit of this S-shaped curve is associated with negligible influence of the semiconductor load on the band gap position and the upper limit is associated with the saturation of influence of this load. This phenomenon is similar to the influence of the approaching metallic shield on MSSW [6]. Also, the non-transmission band positions corresponding to the resonances of different orders is observed in the model at different electron density in GaAs. These differences may be explained, for example, by uneven distribution of electron density in the experiment (due to different laser beam intensity and complex electron distribution over the sample thickness due to diffusion), finite length of the GaAs plate in the studied sample and inhomogeneous interaction between the electromagnetic field of the MSSW multimode wave process [32,34,36] and semiconductor load.

3. Conclusion

The study has demonstrated that optical formation of non-transmission bands of the magnon crystal based on the YIG|GaAs lamellar structure is possible. The study was the first to show the MSSW absorption peak growth in such periodic structure by the Brillouin light scattering method. Moreover, comparison of the BLS spectra with the numerically calculated dispersion characteristics of eigenwaves in such structure has shown that the formed non-transmission bands belong to the Bragg resonances of transmitted and reflected MSSW of the studied structure. Growth of non-transmission band widths and signal absorption enhancement in them is associated with the contrast enhancement of the semiconductor periodic lattice with increased power of the optical laser that illuminated the semiconductor. The followed growth of non-transmission band frequency is associated with enhanced MSSW shielding when the density of optically induced electrons is increased that was shown by numerical calculations of dispersion wave characteristics.

The study allows to proceed to periodic lattices of magnon crystals produced only by optical methods with possibility of period variation with time. Also, this structure is potentially scalable to submicron and nanometric sizes taking into account the existing studies regarding growing of such multilayers.

Funding

This study was financially supported by the Russian Science Foundation (project No. 23-29-00610).

Conflict of interest

The authors declare that they have no conflict of interest.

References

- [1] A. Barman, G. Gubbiotti, S. Ladak, A.O. Adeyeye, M. Krawczyk, J. Gräfe, C. Adelmann, S. Cotofana, A. Nacemi, V.I. Vasyuchka, B. Hillebrands, S.A. Nikitov, H. Yu, D. Grundler, A.V. Sadovnikov, A.A. Grachev, S.E. Sheshukova, J.-Y. Duquesne, M. Marangolo, G. Csaba, W. Porod, V.E. Demidov, S. Urazhdin, S.O. Demokritov, E. Al-bisetti, D. Petti, R. Bertacco, H. Schultheiss, V.V. Kruglyak, V.D. Poimanov, S. Sahoo, J. Sinha, H. Yang, M. Münzenberg, T. Moriyama, S. Mizukami, P. Landeros, R.A. Gallardo, G. Carlotti, J.-V. Kim, R.L. Stamps, R.E. Camley, B. Rana, Y. Otani, W. Yu, T. Yu, G.E.W. Bauer, C. Back, G.S. Uhrig, O.V. Dobrovolskiy, B. Budinska, H. Qin, S. van Dijken, A.V. Chumak, A. Khitun, D.E. Nikonov, I.A. Young, B.W. Zingsem, M. Winklhofer. *J. Phys.: Condens. Matter* **33**, 41, 413001 (2021).
- [2] V.V. Kruglyak, S.O. Demokritov, D. Grundler. *J. Phys. D* **43**, 26, 264001 (2010).
- [3] S.O. Demokritov, A.N. Slavin. *Magnonics: From Fundamentals to Applications*. Springer Science & Business Media (2012).
- [4] S.A. Nikitov, D.V. Kalyabin, I.V. Lisenkov, A.N. Slavin, Yu.N. Barabanenkov, S.A. Osokin, A.V. Sadovnikov, E.N. Beginin, M.A. Morozova, Yu.P. Sharaevsky, Yu.A. Filimonov, Yu.V. Khivintsev, S.L. Vysotsky, V.K. Sakharov, E.S. Pavlov. *Phys. Usp.* **58**, 10, 1002 (2015).
- [5] D.D. Stancil, A. Prabhakar. *Spin Waves: Theory and Applications*. Springer Science & Business Media (2009).
- [6] A.G. Gurevich, G.A. Melkov. *Magnitnye kolebaniya i volny*. Nauka, M. (1994). 462 p. (in Russian).
- [7] B. Lenk, H. Ulrichs, F. Garbs, M. Münzenberg. *Phys. Rep.* **507**, 4–5, 107 (2011).
- [8] A. Litvinenko, R. Khymyn, V. Tyberkevych, V. Tikhonov, A. Slavin, S. Nikitov. *Phys. Rev. Appl.* **15**, 3, 034057 (2021).
- [9] M. Krawczyk, D. Grundler. *J. Phys.: Condens. Matter* **26**, 12, 123202 (2014).
- [10] A.V. Chumak, A.A. Serga, B. Hillebrands. *J. Phys. D* **50**, 24, 244001 (2017).
- [11] Y.K. Fetisov, A.V. Makovkin. *J. Appl. Phys.* **79**, 8, 5721 (1996).
- [12] B. Obry, V.I. Vasyuchka, A.V. Chumak, A.A. Serga, B. Hillebrands. *Appl. Phys. Lett.* **101**, 19, 192406 (2012).
- [13] A.V. Chumak, T. Neumann, A.A. Serga, B. Hillebrands, M.P. Kostylev. *J. Phys. D* **42**, 20, 205005 (2009).
- [14] Q. Wang, A.V. Chumak, L. Jin, H. Zhang, B. Hillebrands, Z. Zhong. *Phys. Rev. B* **95**, 13, 134433 (2017).
- [15] A.B. Ustinov, A.V. Drozdovskii, A.A. Nikitin, A.A. Semenov, D.A. Bozhko, A.A. Serga, B. Hillebrands, E. Lähderanta, B.A. Kalinikos. *Commun. Phys.* **2**, 1, 137 (2019).
- [16] O.V. Dobrovolskiy, R. Sachser, T. Brächer, T. Böttcher, V.V. Kruglyak, R.V. Vovk, V.A. Shklovskij, M. Huth, B. Hillebrands, A.V. Chumak. *Nature Phys.* **15**, 5, 477 (2019).
- [17] A.V. Sadovnikov, A.A. Grachev, A.A. Serdobintsev, S.E. Sheshukova, S.S. Yankin, S.A. Nikitov. *IEEE Magn. Lett.* **10**, 1, 5506405 (2019).
- [18] Y. Fetisov, A. Makovkin, V. Studenov. In: *International Topical Meeting on Microwave Photonics. MWP'96 Technical Digest. Satellite Workshop (Cat. No 96TH8153)*. IEEE (1996). P. 37–40.
- [19] A.V. Sadovnikov, E.N. Beginin, S.E. Sheshukova, Yu.P. Sharaevskii, A.I. Stognij, N.N. Novitski, V.K. Sakharov, Yu.V. Khivintsev, S.A. Nikitov. *Phys. Rev. B* **99**, 5, 054424 (2019).

- [20] S.V. Eliseeva, D.I. Sementsov, M.M. Stepanov. *Technical Phys.* **78**, 10, 1319 (2008).
- [21] A.S. Kindyak. *Mater. Lett.* **24**, 6, 359 (1995).
- [22] V.D. Bessonov, M. Mruczkiewicz, R. Gieniusz, U. Guzowska, A. Maziewski, A.I. Stognij, M. Krawczyk. *Phys. Rev. B* **91**, 10, 104421 (2015).
- [23] L.V. Lutsev, A.I. Stognij, N.N. Novitskii, V.E. Bursian, A. Maziewski, R. Gieniusz. *J. Phys. D* **51**, 35, 355002 (2018).
- [24] F.G. Bass, A.A. Bulgakov. *Kinetic and Electrodynamic Phenomena in Classical and Quantum Semiconductor Superlattices*. Nova Sci. Publishers, N.Y. (1997).
- [25] D.A. Neamen. *Semiconductor Physics and Devices: Basic Principles*. McGraw-Hill (2003).
- [26] S.O. Demokritov, B. Hillebrands, A.N. Slavin. *Phys. Rep.* **348**, 6, 441 (2001).
- [27] A.G. Gurevich, G.A. Melkov. *Magnetization Oscillations and Waves*. CRC Press (2020).
- [28] M. Sotoodeh, A.H. Khalid, A.A. Rezazadeh. *J. Appl. Phys.* **87**, 6, 2890 (2000).
- [29] G.E. Stillman, C.M. Wolfe, J.O. Dimmock. *J. Phys. Chem. Solids* **31**, 6, 1199 (1970).
- [30] M.H. Weiler. *Semicond. Semimet.* **16**, 119 (1981).
- [31] R.W. Damon, J.R. Eshbach. *J. Phys. Chem. Solids* **19**, 3–4, 308 (1961).
- [32] T.W. O’Keeffe, R.W. Patterson. *J. Appl. Phys.* **49**, 9, 4886 (1978).
- [33] M. Mruczkiewicz, M. Krawczyk. *J. Appl. Phys.* **115**, 11, 113909 (2014).
- [34] A.V. Sadvnikov, K.V. Bublikov, E.N. Beginin, S.E. Sheshukova, Yu.P. Sharaevskii, S.A. Nikitov. *JETP Lett.* **102**, 3, 142 (2015).
- [35] A.S. Kindyak. *ZhTF* **69**, 6, 119 (1999). (in Russian).
- [36] A.V. Sadvnikov, E.N. Beginin, K.V. Bublikov, S.V. Grishin, S.E. Sheshukova, Y.P. Sharaevskii, S.A. Nikitov. *J. Appl. Phys.* **118**, 20, 203906 (2015).

Translated by Ego Translating